Results from the Pierre Auger Observatory

J. J. Beatty for the Pierre Auger Collaboration
Departments of Physics and Astronomy, The Ohio State University, Columbus, OH 43210, USA

Cosmic rays of energies exceeding 10^{20} eV have been observed. These particles are of special interest because their interactions with the cosmic microwave background limit the distance from which they can propagate, and because they are deflected little by Galactic and extragalactic magnetic fields. These cosmic rays are now being studied using the Pierre Auger Observatory, now operating in Argentina. Auger employs both the air fluorescence and surface detector measurement techniques in a hybrid mode, which facilitates an improved understanding of systematic effects in measuring cosmic ray showers. We report highlights of the first results from Auger, which include a first estimate of the spectrum above 3×10^{18} eV, a search for a localized excess flux from the Galactic center region, and a limit on the primary photon fraction.

1. OVERVIEW

1.1. Scientific Motivation

Cosmic ray particles of enormous energies have been observed. The highest energy cosmic ray showers have energies of tens of joules, about eight orders of magnitude above the highest energies achieved in terrestrial accelerators. The source of these particles and the mechanism by which they are accelerated to such high energies remains a mystery.

As first noted by Greisen [1] and by Zatsepin and Kuz'min [2], cosmic rays with energies above ~5×10^{19} eV interact with the cosmic microwave background. In the rest frame of a sufficiently energetic particle, photons from the cosmic microwave background are blueshifted to gamma ray energies. For protons, this results in photopion production, primarily via the Δ resonance. High-energy nuclei are degraded via giant dipole resonances, and photons experience losses due to electron pair production on the microwave and radio photon backgrounds. This implies that cosmic rays with energy above the threshold for these processes should be strongly suppressed unless they come from closer than about 50 Mpc. This effect is known as the Greisen-Zatsepin-Kuz'min (GZK) cutoff.

Cosmic rays with energies up to about 10^{15} eV can be accounted for by acceleration in the shocks that develop in supernova remnants. However, it is difficult to identify plausible sources for cosmic rays with energies exceeding 10^{20} eV. Hillas [3] discusses the relevant considerations, which include a minimum value of the product of the magnetic field and the radius of the accelerating region. Additional constraints arise due to synchrotron losses for small sources with large magnetic fields and due to GZK losses for large sources. The most promising conventional astrophysical sources are shocks in the jets produced by active galactic nuclei. Exotic alternative 'top-down' scenarios involve production of the highest energy cosmic rays by the decay of GUT-scale relic particles produced in the early Universe [4].

In principle we should be able to locate the source of cosmic ray particles above the GZK cutoff because they experience very little deflection by galactic and intergalactic magnetic fields. Unlike lower energy cosmic rays, their arrival direction should correspond with the direction of the source. The highest energy cosmic rays observed thus far

do not point back to plausible sources or mass concentrations, and the data are consistent with isotropy. Their origin therefore remains a mystery.

Particles at these energies are extremely rare. The flux of particles with energy above 10^{19} eV is only about one per square kilometer per steradian per year. Since the differential spectrum falls approximately as the inverse cube of energy, the flux of particles above 10^{20} eV is about one per square kilometer per steradian per century. A detector with very large aperture is required to make progress on a reasonable timescale. The Pierre Auger Observatory was designed to address this problem.

1.2. Air-shower Measurements and the Hybrid Approach

Cosmic rays with energies up to about 10 TeV can be observed directly by instruments on satellites or balloons. At higher energies it becomes impractical to loft a detector large enough to detect a sufficient number of particles in a reasonable length of time. Above these energies, the Earth's atmosphere can be used as the detector medium. When a high-energy particle strikes the atmosphere, it produces a cascade of particles. At each generation of the cascade, a larger fraction of the energy is transferred from hadronic particles (mostly pions) to electrons and photons. The remaining charged pions decay when their Lorentz factor becomes low enough that decays dominate over interactions. After a few generations, the cascade is nearly completely electromagnetic. When the energy of the electromagnetic particles drops below the critical energy (~100 MeV in air), the cascade begins to diminish as the particles lose energy by ionization.

Measurements of ultrahigh energy cosmic rays have been made using two techniques. Air fluorescence detectors are used to observe the fluorescence of atmospheric nitrogen excited by the charged particles in the shower. The fluorescence light emitted is proportional to the energy deposited in the atmosphere by the shower, which can be calibrated to yield a measurement of the primary particle energy. The light observed on the ground must be corrected for the varying attenuation of the atmosphere and for contamination of the fluorescence signal by Cherenkov light. In addition, fluorescence measurements are practical only on clear moonless nights, resulting in a duty cycle of about 10%.

An array of particle detectors on the Earth's surface can also be used to measure cosmic ray showers. The shower consists particles traveling at nearly the velocity of light distributed in a thin disk oriented perpendicular to the arrival direction of the incident particle. The direction of the shower can be determined to about 1° by measuring the time of arrival of the shower at successive detectors on the ground. The shower energy is determined by analyzing the measured particle density profile.

Each of these techniques has strengths and limitations. A surface detector array operates continuously with a well-defined geometrical aperture for showers well-above threshold. The fluorescence detector aperture is a function of energy, and depends on the duty cycle, cloud cover, brightness of the shower relative to the sky background, and atmospheric clarity at the time of the observations. The fluorescence detector makes a measurement of the shower energy that is in principle nearly calorimetric, and the depth at which the shower maximum occurs is a diagnostic of composition. The surface detector can measure many features of the shower at ground level, including signal density in the chosen detector, the electromagnetic and muon components, and the shape and timing structure of the shower front. These are useful, but their interpretation involves comparison to simulations of shower development that must rely on extrapolations of particle physics to energies beyond those that can be measured in accelerator experiments.

There has been some controversy in recent years concerning the spectrum of the highest energy cosmic rays. The High Resolution Fly's Eye (HiRes) group, which operates a fluorescence experiment, has reported a spectrum that seems to show evidence for GZK suppression of the flux above 6 x 10^{19} eV [5]. The Akeno Giant Air Shower Array (AGASA) collaboration, a surface detector based on scintillation counters, reports a spectrum without evidence of a GZK cutoff [6]. In addition to differences in the spectral shape, there is also a difference in the absolute flux below the GZK cutoff which can be accounted for by a ~20% difference in the energy scale calibration between the two experiments. This difference in energy scale is within the quoted systematic errors. Nevertheless, the controversy over the existence of a spectral feature corresponding to the GZK cutoff remains open.

The Pierre Auger Observatory employs both the surface detector and fluorescence techniques in a hybrid mode. The surface detector operates continuously, and provides a large data sample with a well-defined aperture. On clear dark nights, fluorescence detectors operate in conjunction with the surface detector to provide a sample of events where both fluorescence and surface detector data are available. This hybrid dataset is used to understand systematic effects in both detectors, and provide a more confident understanding of the showers than could be obtained from either technique alone.

2. THE OBSERVATORY

Figure 1 shows the southern observatory layout superimposed on a map of the site. The site is located in Mendoza Province, Argentina near the town of Malargüe. The typical altitude of the site is ~1500 meters. The surface detector array will cover 3000 km^2 using 1600 autonomous detector stations. Four fluorescence detector sites view the atmosphere above the surface detector. The observatory campus in Malargüe includes the central data acquisition facilities, office space, and an assembly area where detectors are prepared for deployment. The surface detector and fluorescence detectors are connected to the central campus through a custom communications network. A northern Auger site has been selected in the United States, near the town of Lamar in southeastern Colorado.

2.1. The Surface Detector

The Auger Observatory's surface particle detectors are water Cherenkov counters. Water Cherenkov detectors are simple and robust, and thus are well suited for the remote and hostile environment of the site. They are sensitive to both the muonic and electromagnetic components of the shower. Each station is a cylindrical water tank with a water volume 3.7 m in diameter and 1.2 m deep, holding 12 metric tons of filtered highly deionized water. Because of the height and volume of the detectors, they are nearly uniformly sensitive to particle tracklength out to very large zenith angles [7]. The water tanks are colored tan to blend in with their surroundings. The water is enclosed within a bag with an inner layer made of white Tyvek, which reflects light diffusely. Three nine-inch photomultiplier tubes detect the Cherenkov light. Signals are extracted from both the anode and the last dynode, with the latter amplified to extend the dynamic range to approximately 10^5. Each signal is filtered using a Bessel filter with a –3dB cutoff at 20 MHz and digitized at 40 MHz using a ten-bit flash ADC. Triggering takes place in an FPGA using the digitized signals. The time of each trigger is determined using a clock on the station that is calibrated against a timing-grade GPS receiver. Event data are read out by a local CPU which performs further event selection, maintains monitoring and calibration

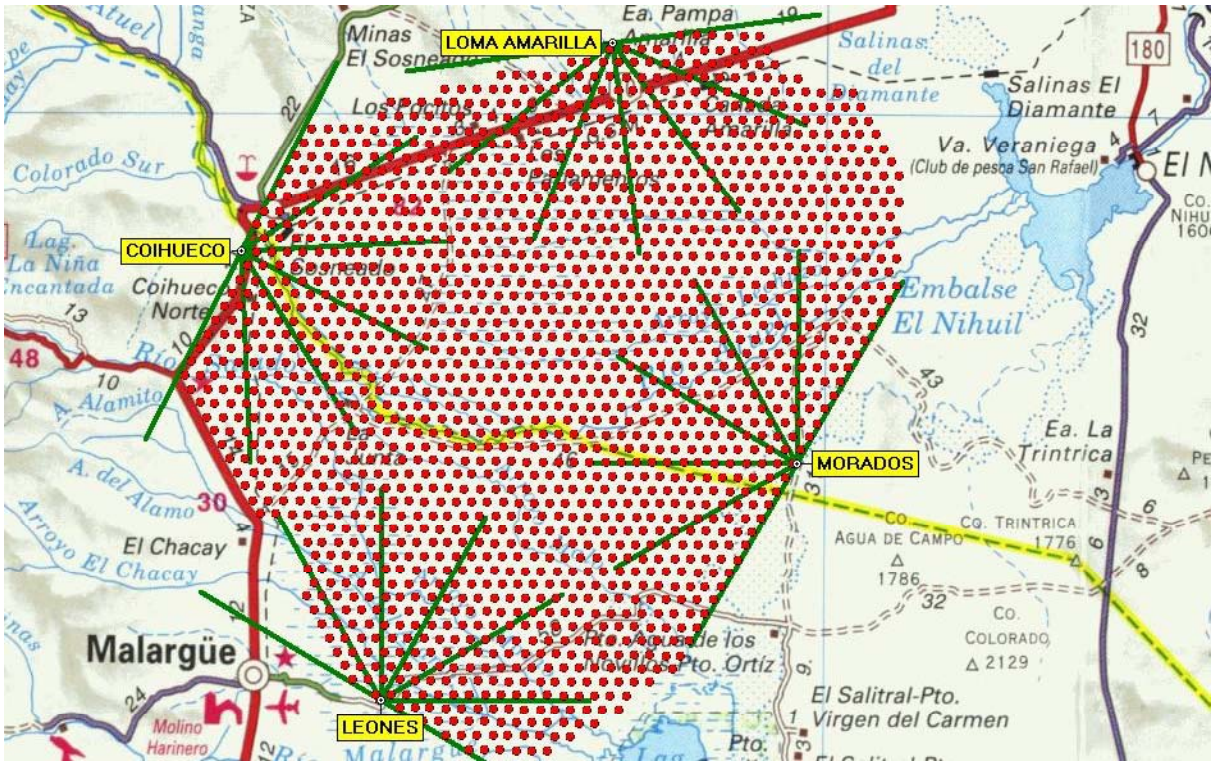

Figure 1: A schematic view of the southern site of the Pierre Auger Observatory, superimposed on a map of the region. The red dots indicate the surface detector locations. The four fluorescence detector sites at Los Leones, Los Morados, Coihueco, and Loma Amarilla are also shown. The green lines pointing from each fluorescence site indicate the directions of the boundaries of the view of each of the six fluorescence telescopes at each site. The observatory campus is located in the town of Malargüe.

data, and communicates with a central data acquisition system (CDAS) using a custom wireless communication system. A solar panel and batteries provide the power to the station, which consumes less than ten watts. The detectors are deployed in a hexagonal grid with a spacing of 1500 meters. Each tank's position is measured using differential GPS, and the station operates its own GPS receiver in position-hold mode, where the known tank position is assumed in solving for the GPS time. This results in a relative precision for the calibrated station clocks of better than 20 ns[8]. Additional details about the surface detector can be found in references [9] and [10].

The surface detector calibration is obtained using cosmic ray muons and low energy showers. The particle density is measured in terms of the charge measured for a vertical and central muon, termed a vertical-equivalent muon (VEM, or Q_{VEM}) . The goal of the calibration procedure is to determine the relationship between Q_{VEM} and electronics channels to good accuracy. Atmospheric muons passing through the tank provide an excellent means for determining Q_{VEM}, as there is a clearly defined peak in a charge histogram [Figure 2] when the tank is triggered using a threefold coincidence at a low threshold. This peak occurs at 1.05 Q_{VEM} in each PMT, as has been measured using a muon telescope with a test tank. When first turned on, each station executes an algorithm that balances the end-to-end gain of the three PMTs at a level that places the peak current for a VEM (I_{VEM}) about 50 channels above baseline. The station then maintains an estimate of the values of Q_{VEM} and I_{VEM} as a function of time. These estimates are used in assessing the health of the detector and in maintaining a stable local trigger. Details of the calibration methods may be found in Reference [11].

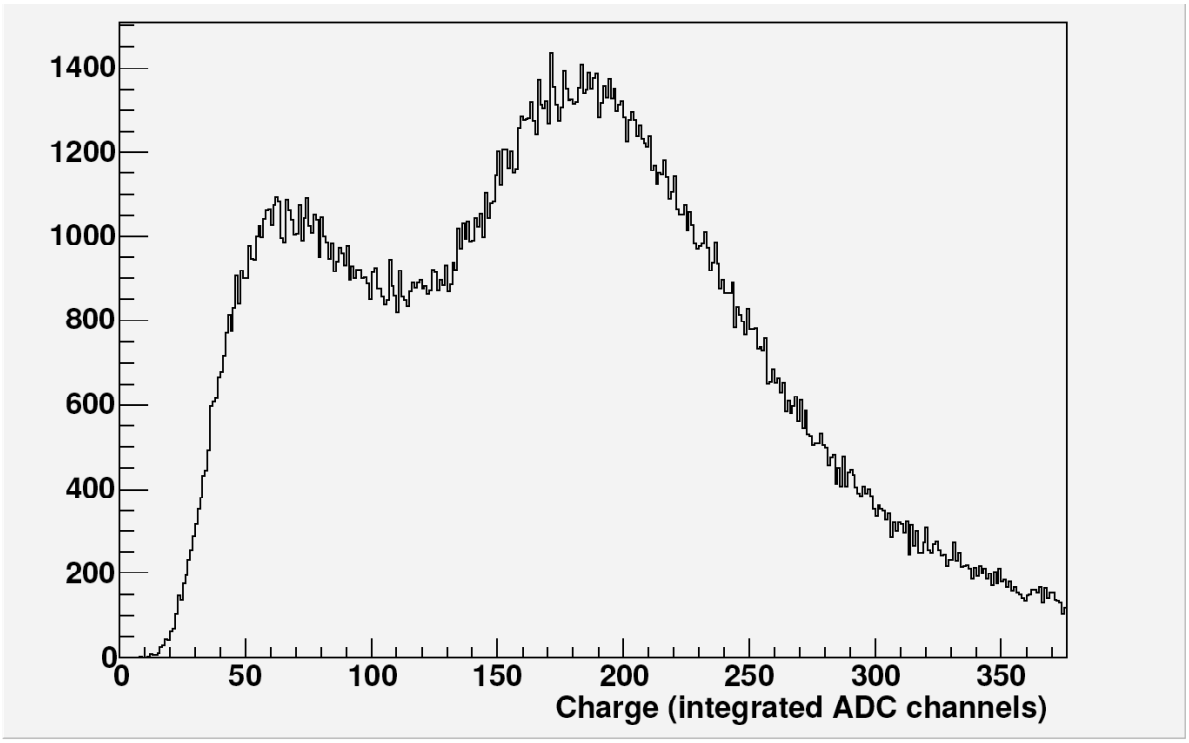

Figure 2: Charge histogram from a surface detector station, triggered by a three-fold coincidence between all 3 PMTs, at a trigger level of five channels above baseline. The first peak is a trigger artifact. The second peak is due to vertical throughgoing atmospheric muons.

The surface detector trigger is hierarchical. The lowest level trigger, T1, is performed by the FPGA in the local station electronics. T1 can be initiated by either of two conditions. The first uses a time-over-threshold (ToT) trigger, which requires that the signal in 13 FADC bins out of a 120 bin window are above a threshold of 0.2 $I_{VEM,est}$ in at least two PMTs, where $I_{VEM,est}$ is the estimated peak current for a vertical equivalent muon obtained by the station's calibration algorithm. The ToT trigger rate averages 1.6 Hz, and is dominated by coincidences of two muons. The ToT trigger is efficient for selecting small signals spread in time such as those produced by distant high-energy showers. A second trigger requires three PMTs have a signal of greater than 1.75 $I_{VEM,est}$ in coincidence. This trigger has a rate of about 100 Hz, and it is needed to detect fast signals (< 200 ns) corresponding to the muonic component generated by horizontal showers. All events that meet either of the T1 trigger conditions are temporarily stored on the station for possible readout. The T2 trigger is applied in the station controller to select from the T1 signals those likely to have come from EAS and to reduce to about 20 Hz the rate of events to be sent to the central station. All ToT triggers are directly promoted T2 whereas T1 threshold triggers are requested to pass a higher threshold of 3.2 $I_{VEM,est}$ in coincidence for 3 PMTs. A timestamp for each T2 trigger is sent to the central data acquisition system (CDAS) at the central campus using the wireless network. The timestamp is accompanied by an indication of whether the ToT or the threshold T2 trigger was satisfied.

The next level trigger, T3, is formed at CDAS by searching for space-time clusters of T2 triggers. Two types of clusters are selected. The first, 3ToT, requires that a station with a ToT trigger have both at least one nearest neighbor

and one additional nearest or second-nearest neighbor, both of which also have a ToT trigger. About 90% of events selected by the 3ToT trigger are showers, and this trigger is most efficient for vertical showers. The rate of 3ToT triggers is about 600 events per day as of mid-2005, or 1.3 events/day per triangle of three operating stations. The other T3 trigger requires a four-fold coincidence of any type of T2 trigger with a less restrictive compactness requirement; one of the four stations may be as much as 6 km away from the others within an appropriate time window. This trigger is absolutely needed to allow for the detection of horizontal showers that generate fast signals and have wide-spread patterns. This trigger selects about 400 events per day, but only 2% are real showers. When CDAS determines that T3 has been satisfied, a request is broadcast to the local stations requesting full readout of events meeting either T2 or T1 and coincident with the T3 time. The data from the stations is accompanied by current calibration data, including raw histograms used to assess the calibration Such a request can also be generated from the fluorescence detector, which extends the hybrid dataset below the threshold for the surface detector to self-trigger. Further details concerning the surface detector trigger and its stability may be found in reference [12].

2.2. The Fluorescence Detector

The fluorescence detectors are distributed in four stations around the perimeter of the surface detector array, and view the atmosphere above the array on moon-less or partially moon-lit nights. As of mid-2005 three of the four fluorescence sites have been completed and are in operation. Two of them, Los Leones and Coihueco, have been collecting data since January 2004, with Los Morados beginning data taking in March 2005. The fourth site at Loma Amarilla will be in operation in the second half of 2006. A fluorescence site contains six identical fluorescence telescopes. Fluorescence light enters the telescope through a 1.10 m radius diaphragm, and light is collected by a 3.5x3.5 m spherical mirror and focused onto a photo-multiplier (PMT) camera. The camera contains 440 hexagonal 45 mm PMTs. Each PMT covers a 1.5° diameter region of the sky. The optical spot size on the focal surface has a diameter of approximately 15 mm (equivalent to 0.5°) for all directions of incoming light. To reduce signal losses when the light spot crosses PMT boundaries, small light reflectors ("Mercedes stars") are placed between PMTs. The field of view of a single telescope covers 30° in azimuth and 28.6° in elevation. The fluorescence telescopes have been installed with an uncertainty of 0.1° in their nominal pointing directions. However, observations of stars crossing the field of view of the telescopes can improve this precision, to 0.01°. An optical filter matched to the fluorescence spectrum (approximately 300 nm to 400 nm) is placed over the telescope diaphragm to reduce night-sky noise. In addition, the diaphragm contains an annular corrector lens as part of the Schmidt telescope design, with an inner radius of 0.85 m and outer radius of 1.10 m. The effect of the lens is to allow an increase in the radius of the telescope diaphragm from 0.85 m to 1.1 m (increasing the effective light collecting area by a factor of two) while maintaining an optical spot size of 0.5° [13].

One of the goals of the FD is to measure air shower energies with an uncertainty smaller than 15%. In order to achieve this goal the fluorescence detectors have to be calibrated with a precision of about 8% and the calibration stability needs to be monitored on a regular basis. An absolute calibration of each telescope is performed three or four times a year, and relative calibrations are performed every night during detector operation. To perform an absolute end-to-end calibration of a telescope, a large homogeneous diffuse light source was constructed for use at the front of the telescope diaphragm. The ratio of the light source intensity to the observed signal for each PMT gives the required

calibration. At present, the precision in the PMT calibration using the source is about 12% [14]. For relative calibration, optical fibers bring light signals to three different diffuser groups for each telescope The total charge per pixel is measured with respect to reference measurements made at the time of absolute calibrations. This allows the monitoring of short and long term stability, the relative timing between pixels and the relative gain of each pixel [15]. The relative calibration information is not yet incorporated in the reconstruction system. However, the average detector stability has been measured and a corresponding systematic uncertainty of 3% has been introduced to account for this. This contributes to the overall 12% systematic uncertainty in the FD calibration. Crosschecks of the FD calibration can be made by reconstructing the energy of laser beams that are fired into the atmosphere from various positions in the SD array. A Central Laser Facility (CLF) located at the center of the array can fire a laser beam into to the sky with known geometry and energy. The observed difference between the reconstructed energy and the real laser energy is of the order of 10% to 15% [16], consistent with the current level of uncertainty in calibrations and knowledge of the atmosphere.

As part of the reconstruction process, the detected light at the telescope must be transformed into the amount of fluorescence light emitted at the shower axis as a function of atmospheric depth. For this it is necessary to have a good knowledge of local atmospheric conditions. We need to account for both Rayleigh and aerosol scattering of light between the shower and the detector, so we must understand the distribution of aerosols and the density of the atmosphere at different heights. In addition, the temperature distribution with height is needed since the fluorescence light yield is a (slow) function of temperature. Finally, the detector volume must be monitored for the presence of clouds. Aerosols in the atmosphere consist of clouds, smoke, dust and other pollutants. The aerosol conditions can change rapidly and are known to have a strong effect on the propagation of fluorescence light. The Observatory has an extensive network of atmospheric monitoring devices. These include LIDAR (a self-contained laser backscattering measuring system), cloud cameras and star monitors. We have also deployed systems to monitor the wavelength dependence and differential scattering properties of the aerosols. More details of these systems can be found in [17]. Presently, only the aerosol information obtained from observing the laser tracks is incorporated in the shower energy reconstruction algorithm. The uncertainty in the currently applied monthly atmospheres in the Auger reconstruction introduce an uncertainty in the atmospheric depth at ground of about 5 g/cm^2[10]. The resulting fluorescence light at the shower track is converted to the energy deposited by the shower by applying the expected fluorescence efficiency at each depth. More details about the FD calibration and performance can be found in [9, 18] and references therein. The estimated systematic uncertainty in the reconstructed shower energy is currently 25%, with activity underway to reduce this significantly.

2.3. Hybrid Operation

A hybrid event is an air shower that is simultaneously detected by the fluorescence detector and the ground array. Data are recovered from both detectors whenever either system is triggered. If an air shower independently triggers both detectors the event is tagged accordingly. There are cases where the fluorescence detector, having a lower energy threshold, promotes a sub-threshold array trigger. Surface stations are matched by timing and location. This is an important capability because these subthreshold hybrid events would not have triggered the array otherwise. The Observatory started operation in hybrid production mode in January, 2004. Surface stations have a 100% duty cycle,

while fluorescence eyes can only operate on clear moonless nights. Both surface and fluorescence detectors have been running simultaneously 14% of the time. The number of hybrid events represents 10% the statistics of the surface array data. A hybrid detector has excellent capability for studying the highest energy cosmic ray air showers. Much of its capability stems from the accurate geometrical reconstructions it achieves. Timing information from even one surface station can much improve the geometrical reconstruction of a shower over that achieved using only eye pixel information. The axis of the air shower is determined by minimizing a χ^2 function involving data from all triggered elements in the eye and at ground. The reconstruction accuracy is better than the ground array counters or the single eye could achieve independently [18, 28]. Using the timing information from the eye pixels together with the surface stations, a core location resolution of 50 m is achieved. The resolution for the arrival direction of cosmic rays is 0.6º [28]. More details about the hybrid performance of the Auger Observatory can be found in [9, 19] and references therein.

Due to its angular accuracy, the hybrid data sample is ideal for anisotropy studies and it will become important for this purpose as greater statistics are accumulated. Many ground parameters, like the shower front curvature and thickness, have always been difficult to measure experimentally, and have usually been determined from Monte Carlo simulation. The hybrid sample provides a unique opportunity in this respect. As mentioned, the geometrical reconstruction can be done using only one ground station, and all the remaining detectors can be used to independently measure the shower characteristics. The possibility of studying the same set of air showers with two independent methods is valuable in understanding the strengths and limitations of each technique. The hybrid analysis benefits from the calorimetric nature of the fluorescence technique and the uniformity of the surface detector aperture.

3. HIGHLIGHTS OF RESULTS

3.1. A First Estimate of the Cosmic Ray Spectrum above 3 EeV

The data for this analysis are from 1 Jan 2004 through 5 Jun 2005. The event acceptance criteria and exposure calculation are described in separate papers [12, 20]. Events are included for zenith angles 0-60°, and results are reported for energies above 3 EeV (3525 events). The array is fully efficient for detecting such showers, so the acceptance at any time is the simple geometric aperture. The cumulative exposure adds up to 1750 km^2 sr yr, which is 7% greater than the total exposure obtained by AGASA [6]. The average array size during the time of this exposure was 22% of what will be available when the southern site of the Observatory has been completed.

Assigning energies to the SD event set is a two-step process. The first step is to assign an energy parameter S_{38} to each event. Then the hybrid events are used to establish the rule for converting S_{38} to energy.

The energy parameter S_{38} for each shower comes from its experimentally measured S(1000), which is the time-integrated water Cherenkov signal S(1000) that would be measured by a tank 1000 meters from the core. S_{38} has the zenith angle dependence of S(1000) removed, and is normalized to the median zenith angle ($\theta \approx 38^o$). The signal S(1000) is attenuated at large slant depths. Its dependence on zenith angle is derived empirically by exploiting the nearly isotropic intensity of cosmic rays. By fixing a specific intensity I_0 (counts per unit of $sin^2\theta$), one finds for each zenith angle the value of S(1000) such that $I(> S(1000)) = I_0$. We calculated a particular constant intensity cut curve

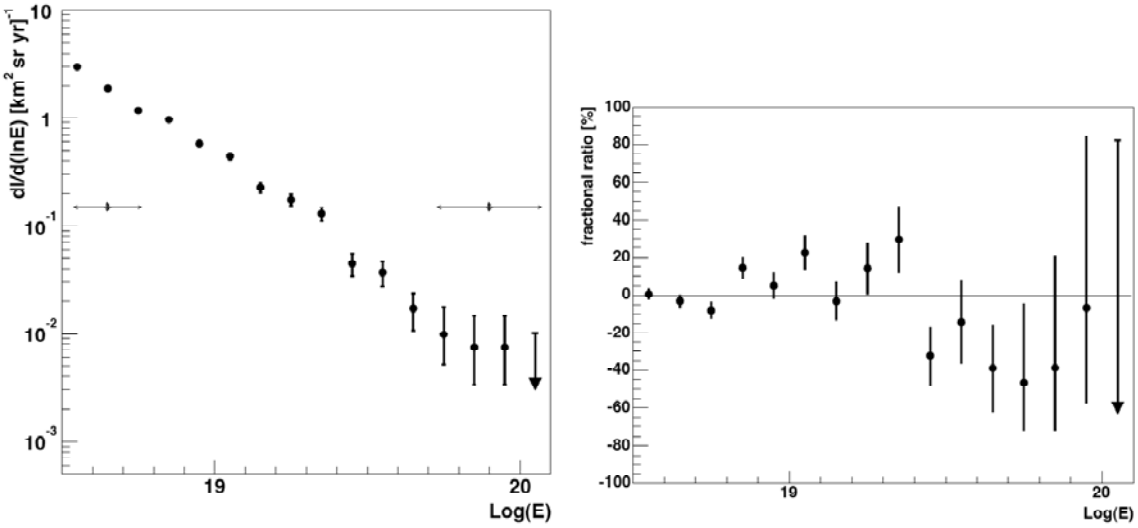

Figure 3: Left : Estimated spectrum. Plotted on the vertical axis is the differential intensity $dI/d\ln E \equiv E(dI/dE)$. Error bars on points indicate statistical uncertainty (or 95% CL upper limit). Systematic uncertainty is indicated by double arrows at two different energies. Right: Percentage deviation from the best-fit power law: $100\times((dI/d(lnE)-F)/F)$. The fitted function is $F = 30.9\pm1.7\times(E/EeV)^{1.84\pm0.03}$. The chisquare per degree of freedom in the fit is 2.4

$CIC(\theta)$ relative to the value at the median zenith angle. Given S(1000) and θ for any measured shower, the energy parameter S_{38} is defined by $S38 \equiv S(1000)/CIC(q)$. It may be regarded as the S(1000) measurement the shower would have produced if it had arrived 38º from the zenith. S_{38} is well correlated with the FD energy measurements in hybrid events that are reconstructed independently by the FD and SD. A linear relation was fitted and gives an empirical rule for assigning energies (in EeV) based on $S38$ (in VEM):

$$E = 0.16\times S_{38}^{1.06} = 0.16\times[S(1000)/CIC(\theta)]^{1.06}.$$

The uncertainty in this rule is discussed below. The distribution over $ln(E)$ produced by this two-step procedure becomes the energy spectrum [Figure 3] after dividing by the exposure, 1750 km^2 sr yr. (See also http://www.auger.org/icrc2005/spectrum.html.)

The Auger Observatory will measure the spectrum over the southern sky accurately in coming years. The spectrum in Figure 3 is only a first estimate. It has significant systematic and statistical uncertainties. The indicated statistical error for each point comes directly from the Poisson uncertainty in the number of measured showers in that logarithmic energy bin. Systematic and statistical uncertainties in S(1000) are discussed elsewhere [21]. There is larger systematic uncertainty in the conversion of S_{38} to energy. Part of that comes from the FD energies themselves. Laboratory measurements of the fluorescence yield are uncertain by 15%, and the absolute calibration of the FD telescopes is presently uncertain by 12%. Together with other smaller FD uncertainties, the total systematic uncertainty in the FD energy measurements is estimated to be 25%. Combining in quadrature the FD systematic uncertainty and this correlation uncertainty, the total systematic energy uncertainty grows from 30% at 3 EeV to 50% at 100 EeV. Horizontal double arrows in Figure 3 indicate this uncertainty, and vertical arrows indicate a 10% systematic uncertainty in the exposure. Additional details of this analysis can be found in [22] and references therein.

The Pierre Auger Observatory is still under construction and growing rapidly. In mid-2007, its cumulative exposure will be approximately seven times greater. The statistical errors will shrink accordingly, permitting a search in the southern skies for spectral features, including the predicted GZK suppression. The enlarged hybrid data set will reduce systematic uncertainty in the FD normalization of the SD energies. Numerous laboratory experiments are attempting to reduce the systematic uncertainty in the fluorescence yield, which will be the dominant uncertainty in the FD normalization of the Auger energy spectrum. The FD detector calibration uncertainty will also be reduced.

3.2. Anisotropy Studies of the Galactic Center region

The galactic center (GC) region is an attractive target for anisotropy studies with the Pierre Auger Observatory. Past observations by the AGASA [23] and SUGAR [24] collaborations indicate an excess of cosmic rays from this region in the EeV energy range. Since the GC harbors a accreting massive black hole, Sgr A* [25,26], it is a natural candidate for a cosmic ray accelerator.

In this study Auger data from January 1, 2004 until June 6, 2005 was used. Events from the surface detector that passed the 3-fold or the 4-fold data acquisition triggers and satisfying our high level physics trigger (T4) and our quality trigger (T5) [27] were selected. The T5 selection is independent of energy and ensures a better quality for the event reconstruction. This data set has an angular resolution better than 2.2º for all of the 3-fold events (regardless of the zenith angle considered) and better than 1.7º for all events with multiplicities > 3 SD stations [28]. In all our analyses the zenith angle was cut at 60º like AGASA, while SUGAR used all zenith angles. To estimate the coverage map, needed to construct excess and excess probability maps, a shuffling technique was used. In Figure 4A the coverage map obtained from our SD sample in a region around the GC is presented. In Figure 4 B, C and D we present the chance probability distributions (mapped to positive Gaussian significance for excesses and negative for deficits) in the same region for various filtering and energy cuts corresponding to our various searches. In these maps the chance probability distributions are consistent with those expected as a result of statistical fluctuations from an isotropic sky.

Regarding the region where the AGASA excess was reported, the results from the Auger Observatory are 1155 events observed, and 1160.7 expected (ratio 1.00±0.03) for the energy range [1.0-2.5] EeV. These results do not support the excess observed by AGASA, and in particular not at the level of 22% as was reported, which would correspond to a 7.5 σ excess. In a worst-case scenario in which the source would be protons and the background much heavier (e.g. iron), the difference in detection efficiency of the Auger trigger at 1 EeV would reduce the sensitivity to a source excess. However, using the Fe/proton efficiency ratio at 1 EeV (70%/50% = 1.44, an upper bound in the range [1-2.5] EeV) a 5.2 σ event excess would still be expected in our data set.

Regarding the excess claimed by SUGAR, we find in their angular/energy window 144 events observed, and 150.9 expected (ratio 0.95±0.08), and hence with over an order of magnitude more statistics we are not able to confirm this claim.

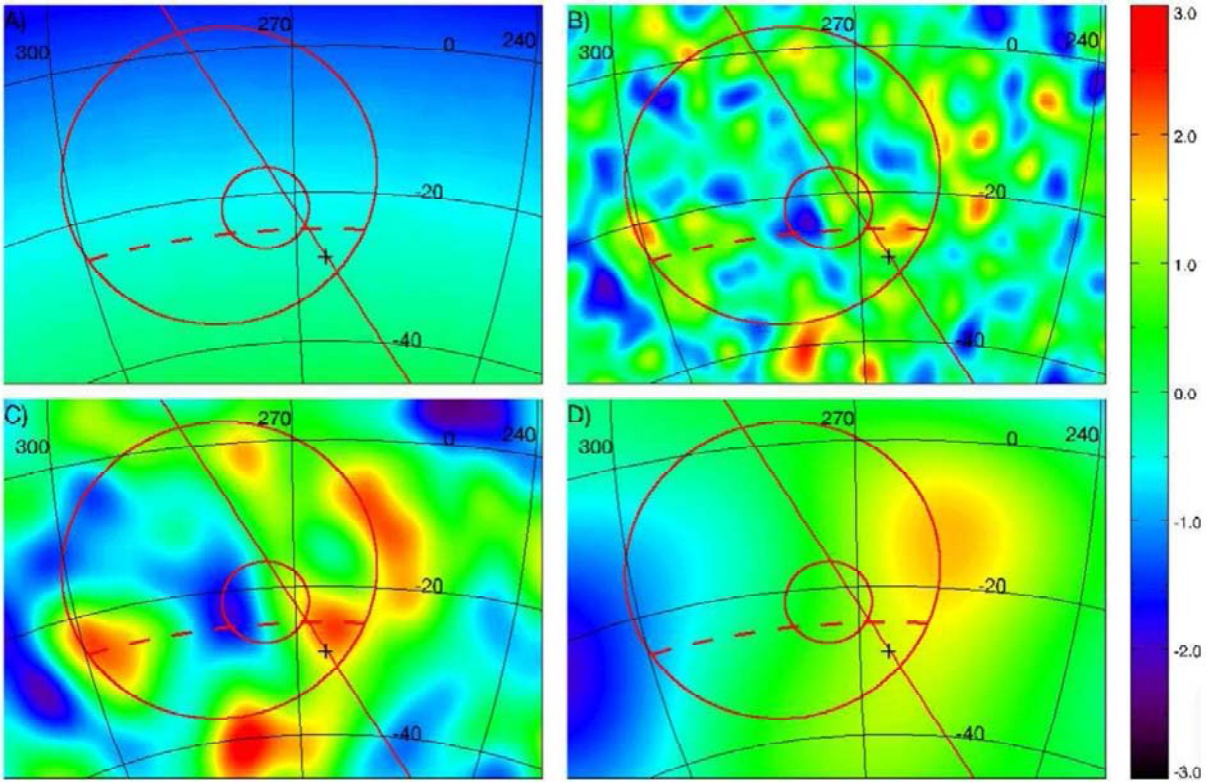

Figure 4: Lambert projections of the galactic centre region, GC (cross), galactic plane (solid line), regions of excess of AGASA and SUGAR (circles), AGASA f.o.v. limit (dashed line). A) coverage map (same color scale as the significance maps, but in a range [0-1.0]). B) significance map in the range [0.8-3.2] EeV smoothed using the individual pointing resolution of the events and a 1.5º filter (Auger-like excess), C) same smoothed at 3.7º (SUGAR-like excess), D) in the range [1.0-2.5] EeV smoothed at 13.3º (AGASA-like excess). Auger has detected no evidence for the previously reported excess fluxes from the Galactic center region.

A search was performed for signals of a point-like source in the direction of the GC using a 1.5º Gaussian filter corresponding to the angular resolution of the SD [28]. In the energy range [0.8–3.2] EeV, we obtain 24.3 events observed and, 23.9 expected (ratio 1.0±0.1). A 95% CL upper bound on the number of events coming from a point source in that window is $n_s(95\%) = 6.7$. This bound can be translated into a flux upper limit (Φ_s) integrated in this energy range. In the simplest case in which the source has a spectrum similar to the one of the overall CR spectrum ($dN/dE \propto E^{-3}$), $\Phi_s = n_s \Phi_{CR} 4\pi\sigma^2 / n_{exp}$ where σ is the size of the Gaussian filter used. Using $\Phi_{CR}(E) = 1.5\ \xi\ (E/EeV)^{-3} \times 10^{-12}$ ($EeV^{-1}\ m^{-2}\ s^{-1}\ sr^{-1}$) where $\xi \in [1, 2.5]$ denotes our uncertainty on the absolute CR flux (ξ is around unity for Auger and 2.5 for AGASA), introducing ε the Iron/proton detection efficiency ratio ($1 < \varepsilon < 1.6$ for $E \in [0.8, 3.2]$ EeV) and, integrating in that energy range we obtain

$$\Phi_s < 2.6\ \xi\ \varepsilon \times 10^{-15} m^{-2} s^{-1} \text{ @ 95\% CL.}$$

In a worst-case scenario, where both ξ and ε take their maximum value, the bound is $\Phi_s = 10.6 \times 10^{-15} m^{-2} s^{-1}$, and still excludes the neutron source scenario suggested in [23, 29] to account for the AGASA excess, or in [30, 31] in connection with the HESS measurements. More details about the GC anisotropy studies with the Auger Observatory data can be found in [32].

3.3. An Upper Limit on the Primary Photon Fraction

A limit on photons in the high energy cosmic rays is useful in constraining 'top-down' models of their origin[4]. The photon upper limit derived here is based on the direct observation of the longitudinal air shower profile and makes use of the hybrid detection technique: the depth of shower maximum, $X_{\max}$, is used as discriminant observable. The information from triggered surface detectors in hybrid events considerably reduces the uncertainty in shower track geometry. The data are taken with a total of 12 fluorescence telescopes [4], situated at two different telescope sites, during the period January 2004 to April 2005. The number of deployed surface detector stations [2] grew from 200 to 800 during this time. For the analysis, hybrid events were selected, i.e. showers observed both by (at least one) surface tank and telescope [19]. Even for one triggered tank only, the additional timing constraint allows a significantly improved geometry fit to the observed profile which leads to a reduced uncertainty in the reconstructed $X_{\max}$.

The reconstruction is based on an end-to-end calibration of the fluorescence telescopes [14], on monitoring data of local atmospheric conditions [17,33], and includes an improved subtraction of Cherenkov light [34] and reconstruction of energy deposit profiles for deriving the primary energy. In total, 16 events with energies above 10^{19} eV are selected. The total uncertainty $\Delta X_{\max}$ of the reconstructed depth of shower maximum is composed of several contributions that, in general, vary from event to event. A conservative estimate of the current $X_{\max}$ uncertainties gives $\Delta X_{\max}$~40 g cm^{-2}. Among the main contributions, each one in general well below $\Delta X_{\max}$ =15 g cm^{-2}, are the statistical uncertainty from the profile fit, the uncertainty in shower geometry, the uncertainty in atmospheric conditions such as the air density profile, and the uncertainty in the reconstructed primary energy, which is taken as input for the primary photon simulation. For each event, high-statistics shower simulations are performed for photons for the specific event conditions. A simulation study of the detector acceptance to photons and nuclear primaries has been conducted. For the chosen cuts, the ratio of the acceptance to photon-induced showers to that of nuclear primaries (proton or iron nuclei) is $\varepsilon = 0.88$. A corresponding correction is applied to the derived photon limit. Fig. 5 shows as an example an event of 11 EeV primary energy observed with $X_{\max}$ = 744 g cm^{-2}, compared to the corresponding $X_{\max}$ distribution expected for primary photons. With $\langle X^{\gamma}_{\max} \rangle$=1020 g cm^{-2}, photon showers are on average expected to reach maximum at depths considerably greater than observed. Shower-to-shower fluctuations are large due to the LPM effect (r.m.s. of 80 g cm^{-2}) and well in excess of the measurement uncertainty. For all 16 events, the observed $X_{\max}$ is well below the average value expected for photons. The $X_{\max}$ distribution of the data is also displayed in Fig. 5. More details about this analysis can be found in [35]. The statistical method for deriving an upper limit follows that introduced in [36]. For the Auger data sample, an upper limit on the photon fraction of 26% at a confidence level of 95% is derived. In Fig. 5, this upper limit is plotted together with previous experimental limits and some estimates based on non-acceleration models. The presented 26% limit confirms and improves the existing limits above 10^{19} eV.

4. SUMMARY

It is important to note that the Pierre Auger Observatory is under construction and that results are preliminary. Growing rapidly, its cumulative exposure will be approximately seven times greater than used for the results reported

here by mid-2007. The statistical errors on our results will shrink accordingly, permitting a search in the southern skies for spectral features, including the predicted GZK suppression, cosmic rays sources as well as primary identification.

It is already clear that the combination of fluorescence and ground array measurements provides reconstruction of the geometry of the shower with much greater accuracy than is achieved with either detector system on its own. Unprecedented core location and direction precision leads to excellent energy and shower development measurements. The enlarged hybrid data set will also reduce systematic uncertainty in the FD normalization of the SD energies.

Acknowledgments

The National Science Foundation, the Department of Energies, and other funding agencies from the collaborating countries have supported this work. The author gratefully acknowledges the support of the National Science Foundation under grant PHY-0457034.

References

[1] K. Greisen, "End to the Cosmic Ray Spectrum?" *Phys. Rev. Lett*. **16**, 748 (1966).
[2] G.T. Zatsepin and V.A. Kuz'min. "Upper Limit of the Spectrum of Cosmic Rays." *JETP Letters* **4**, 78 (1966).
[3] A. M. Hillas, "The Origin of Ultra-High-Energy Cosmic Rays." *Ann. Rev. Astron. Astrophys.* **22**, 425 (1984).
[4] G. Gelmini, O. Kalashev, and D.V. Semikoz. "GZK Photons as Ultra High Energy Cosmic Rays." [astro-ph/0506128] and references therein.
[5] R.U. Abbasi et al. (High Resolution Fly's Eye Collaboration). "Observation of the Ankle and Evidence for a High-Energy Break in the Cosmic Ray Spectrum." *Phys Lett.* **B619**, 271 (2005).
[6] M. Takeda et al. (AGASA Collaboration). "Energy Determination in the Akeno Giant Air Shower Array experiment." *Astropart. Phys.* **19**, 447 (2003).
[7] M. Aglietta et al. for the Auger Collaboration. "Response of the Pierre Auger Observatory Water Cherenkov Detectors to Muons." *Proc. 29th Internat. Cosmic Ray Conf. (Pune)*, (2005).
[8] P. Allison et al. for the Auger Collaboration. "Timing calibration and synchronization of surface and fluorescence detectors of the Pierre Auger Observatory." *Proc. 29th Internat. Cosmic Ray Conf. (Pune),* (2005).
[9] J.Abraham et al (Auger Collaboration). "Properties and performance of the prototype instrument for the Pierre Auger Observatory." *Nucl. Instr. Meth.* **A523**, 50 (2004).
[10] X. Bertou for the Auger Collaboration, "Performance of the Pierre Auger Observatory Surface Detector." *Proc. 29th Internat. Cosmic Ray Conf. (Pune)*, (2005). [astro-ph/0508466]
[11] M. Aglietta et al. for the Auger Collaboration. "Calibration of the surface array of the Pierre Auger Observatory." *Proc. 29th Internat. Cosmic Ray Conf. (Pune)*, (2005).
[12] D. Allard et al. for the Auger Collaboration. "The trigger system of the Pierre Auger Surface Detector: operation, efficiency, and stability." *Proc. 29th Internat. Cosmic Ray Conf. (Pune)*, (2005). [astro-ph/0510320]
[13] R. Sato and C. Escobar for the Auger Collaboration. "The performance of the corrector lenses for the Auger fluorescence detector." *Proc. 29th Internat. Cosmic Ray Conf. (Pune)*, (2005).
[14] P. Bauleo *et al.* for the Auger Collaboration, "Absolute calibration of the Auger fluorescence detectors." *Proc. 29th Internat. Cosmic Ray Conf. (Pune)*, (2005).
[15] C. Aramo et al. for the Auger Collaboration. "Optical relative calibration and stability monitoring for the Auger fluorescence detector." *Proc. 29th Internat. Cosmic Ray Conf. (Pune),* (2005). [astro-ph/0507577]
[16] F. Arqueros et al. for the Auger Collaboration, "The Central Laser Facilty at the Pierre Auger Observatory." *Proc. 29th Internat. Cosmic Ray Conf. (Pune),* (2005). [astro-ph/0507334]
[17] R. Cester et al. for the Auger Collaboration. "Atmospheric aerosol monitoring at the Pierre Auger Observatory." *Proc. 29th Internat. Cosmic Ray Conf. (Pune),* (2005).
[18] J. Bellido for the Auger Collaboration, "Performance of the Fluorescence Detectors of the Pierre Auger Observatory." *Proc. 29th Internat. Cosmic Ray Conf. (Pune)*, (2005). [astro-ph/0508389]
[19] M. Mostafa for the Auger Collaboration, "Hybrid performance of the Pierre Auger Observatory." *Proc. 29th Internat. Cosmic Ray Conf. (Pune)*, (2005).

[20] D. Allard et al. for the Auger Collaboration, "Aperture calculation of the Pierre Auger Observatory surface detector." *Proc. 29th Internat. Cosmic Ray Conf. (Pune)*, (2005). [astro-ph/0511104]
[21] P. Ghia for the Auger Collaboration, "Statistical and systematic uncertainties in the event reconstruction and S(1000) determination by the Pierre Auger Surface Detector." *Proc. 29th Internat. Cosmic Ray Conf. (Pune)*, (2005). [astro-ph/0507029]
[22] P. Sommers for the Auger Collaboration. "First estimate of the primary cosmic ray energy spectrum above 3 EeV from the Pierre Auger Observatory" *Proc. 29th Internat. Cosmic Ray Conf. (Pune)*, (2005). [astro-ph/0507150]
[23] N. Hayashida et al. (AGASA Collaboration). "The anisotropy of cosmic ray arrival direction around 10^{18} eV." *Proc. 26th Internat Cosmic Ray Conf. (Salt Lake City)*, (1999). [astro-ph/9906056]
[24] J.A. Bellido *et al.* "Southern Hemisphere Observations of a 10^{18} eV Cosmic Ray Source." *Astropart. Phys.* **15**,167 (2001). [astro-ph/0009039]
[25] F. Melia and H. Falcke. "The Supermassive Black Hole at the Galactic Center." *Ann Rev. Astron. Astrophys*. **39**, 309 (2001).
[26] R. Narayan, I .Yi, and R. Mahadevan. "Explaining the spectrum of Sagittarius A* with a model of an accreting black hole." *Nature* **374**, 623 (2002).
[27] D. Allard *et al.* for the Auger Collaboration. "The trigger system of the Pierre Auger Surface Detector: operation, efficiency and stability." *Proc. 29th Internat. Cosmic Ray Conf. (Pune)*, (2005).
[28] C. Bonifazi for the Auger Collaboration, "Angular Resolution of the Pierre Auger Observatory." *Proc. 29th Internat. Cosmic Ray Conf. (Pune)*, (2005).
[29] M. Bossa *et al*., "Decaying neutron propagation in the Galaxy and the cosmic ray anisotropy at 1 EeV." *J. Phys G* **29 ,** 1409 (2003).
[30] F. Aharonian *et al.* (HESS Collaboration). "Very high energy gamma rays from the direction of Sagittarius A*." *Astron. Astrophys.* **425**, L13 (2004). [astro-ph/0408145].
[31] F. Aharonian and A.Neronov. "High energy gamma rays from the massive black hole in the Galactic Center." *Astrophys. J*. **619**, 306 (2005). [astro-ph/0408303]
[32] A. Letessier-Selvon for the Auger Collaboration, "Anisotropy studies around the Galactic center at EeV energies with Auger data." *Proc. 29th Internat. Cosmic Ray Conf. (Pune)*, (2005).
[33] B. Keilhauer *et al.* for the Auger Collaboration. "Atmospheric Profiles at the Southern Pierre Auger Observatory and their Relevance to Air Shower Measurement." Proc. 29th Internat. Cosmic Ray Conf. (Pune), (2005). [astro-ph/0507275]
[34] F. Nerling *et al.*, for the Auger Collaboration. "Impact of a new Cherenkov light parametrization on the reconstruction of shower profiles from Auger hybrid data." Proc. 29th Internat. Cosmic Ray Conf. (Pune), (2005).
[35] M. Risse for the Auger Collaboration. "Upper limit on the primary photon fraction from the Pierre Auger Observatory." Proc. 29th Internat. Cosmic Ray Conf. (Pune), (2005). [astro-ph/0507402]
[36] M. Risse *et al.*, "Upper limit on the photon fraction in highest energy comsic rays from AGASA data." *Phys Rev. Lett.* **95** 171102 (2005). [astro-ph/0502418]